Evaluation of Performance of Dedicated, Compact Scintillation Cameras

D.P. McElroy[1], E.J. Hoffman[1], L. MacDonald[2], B.E. Patt[2], J.S. Iwanczyk[2], Y. Yamaguchi[2] and C.S. Levin[3]

[1]UCLA School of Medicine, Division of Nuclear Medicine and Biophysics, Los Angeles CA 90095 USA

[2]Gamma Medica, Division of Photon Imaging, Inc., 19355 Business Center Drive, Suite 8, Northridge, CA 91324.

[3]UCSD/VA Medical Centers, 3350 La Jolla Village Drive, San Diego, CA 92161

Abstract

As part of the development of dedicated scintillation cameras, we compared the performances of 2 dedicated cameras with a standard clinical camera (Siemens Orbiter). One dedicated camera was based on a single Position Sensitive Photomultiplier (PSPMT) coupled to a 6 cm by 6 cm by 6 mm NaI(Tl) crystal and the other was based on multiple-PSPMTs coupled to a 2 mm by 2 mm by 6 mm matrix of NaI(Tl) crystals.

Spatial resolution was measured with all cameras as a function of depth. The ability of the cameras to measure small superficial tumors was tested with a phantom consisting of 6 hot cylindrical tumors of height 3 mm and varying diameters against a warm background. The tumors were imaged at various depths within the background using tumor to background activity concentration ratios of 10:1 and 5:1.

The dedicated cameras show improved performance in imaging the breast tumor phantom, suggesting that these devices will have a role in scintimammography and assisting in O.R. procedures such as sentinel node dissection and other shallow depth of field applications.

I. Introduction

Although breast cancer is the most frequently occurring form of cancer in American women, it has a high cure rate if found in its earliest stages (95% 5 year survival). X-ray mammography has become the method of choice for detecting early signs of breast cancer, for it has a very high diagnostic sensitivity (80% - 90%). In addition, it is inexpensive and is readily available, making it an ideal screening tool. X-ray mammography shows reduced diagnostic sensitivity, however, in women with dense breasts. It also suffers from poor specificity (10% - 35%), particularly for non-palpable tumors, leading to a large number of unnecessary biopsies. In an attempt to reduce this number, many other imaging modalities, including Positron Emission Tomography (PET), Magnetic Resonance Imaging (MRI) and ultrasound, have tried to address the limitations of mammography and have been used as an adjunct to it in cases where mammograms are inconclusive.

^{99m}Tc-sestamibi (MIBI) is a tracer with high uptake in breast carcinoma compared with normal breast tissue. Studies using MIBI in single photon planar imaging (scintimammography) have shown high diagnostic sensitivities and specificities in the range of 80% - 95% [1]. MIBI can also be used to detect lymph node metastases, and may be particularly important in evaluating the sentinel lymph node [2]. MIBI has the advantage of being both relatively inexpensive and more widely available than FDG PET or MRI, making it an attractive adjunct to mammography in the diagnosis and staging of breast cancer.

Commonly available Anger cameras are not ideal for breast imaging. They are large, bulky and designed for general purpose imaging. Breasts are imaged in the prone lateral position, so lesions located in the medial quadrants of the breast or near the chest wall may escape detection [3]. Also, due to the limited spatial resolution of these cameras, there is a significant decrease in diagnostic sensitivity for non-palpable (less than 1 cm diameter) lesions. In response to these problems, we have developed two compact, dedicated scintillation cameras for breast and sentinel node imaging. They can easily be positioned close to the breast on all sides and can be angled to avoid background radiation from the heart, liver and other organs, or can image the breast while under compression, reducing tumor to collimator distance and scatter. Their collimators are optimized for efficiency and shallow depth of field imaging, showing improved spatial resolution and sensitivity as compared with larger multi-purpose cameras. The dedicated camera is also portable, enabling its use in the mammography suite or in the surgical suite as an aid in locating the sentinel node for biopsy.

Several other groups have been developing small gamma cameras for breast imaging, some based on multiple PSPMTs [4] and others based on a single PSPMT [5] [6]. We have been developing both a small gamma camera based on multiple PSPMTs and a small camera based on a single square PSPMT. In this study we compare the performance of the two dedicated scintillation cameras under development with a standard anger camera in clinical use through their ability to image artificial breast lesions.

II. Materials and Methods

A. *"LumaGem" Dedicated Scintillation Camera*

The LumaGem camera (Gamma Medica Inc., Northridge, CA) [7] consists of a compact 15 cm x 20 cm x 12 cm head attached to a fully articulating arm, which is mounted on a mobile base with on board electronics and computer for image display and processing. It employs an array of discrete 2 mm x 2 mm x 6 mm NaI(Tl) crystals coupled to an array of Position Sensitive Photomultiplier Tubes (PSPMTs), for a total imaging area of 12.8 cm x 12.8 cm. In this study we tested the camera with a matching square hole collimator and with a hexagonal hole collimator consisting of 1.25 mm diameter holes and 0.25 mm thick septa, both of which are 2 cm thick.

B. *Single PSPMT Scintillation Camera*

A small prototype test camera has previously been reported on by Levin et. al. [8] [9] and was evaluated as part of this study. It consists of a single 6 cm x 6 cm x 6 mm NaI(Tl) crystal coupled to a single square 77 x 77 mm^2 Hamamatsu R3941 PSPMT, with a 2 cm thick, 1.5 mm diameter hexagonal hole collimator. Standard CAMAC

0-7803-6503-8/01/$10.00 2001 IEEE

readout electronics are used. Two NaI(Tl) crystals were used as part of the evaluation of this camera; one has black, light absorbing material around its sides with reflective material on the front, and the other white reflective material on all sides.

An in-house linearity correction was also developed for this camera which remedies inherent non-uniformities and non-linearities by correctly placing mispositioned events. Other such corrections have been described in the literature [10] [11] [12]. We chose a method that uses slit source images in orthogonal directions to generate a look up table of position correction factors, which are applied to the data post acquisition.

C. "Orbiter" Multi-Purpose Scintillation Camera

The Siemens Orbiter (Medical Systems, Hoffman Estates, IL) is a large, general purpose scintillation camera in routine clinical use in the UCLA nuclear medicine clinic. Measurements were made with this camera using a low energy, high resolution (LEHR) collimator (2.4 cm thick with 1.13 mm diameter holes). It employs a 45 cm diameter, 9 mm thick NaI(Tl) crystal.

D. Cylindrical Tumor Phantom

An acrylic cylindrical tumor phantom of diameter 6 cm and height 1.2 cm, imbedded with six fillable cylinders of height 3 mm and diameters 2, 3, 4, 5, 6 and 7 mm, was designed to be imaged at several depths (distances to the collimator face) within a warm background and scatter environment consisting of four cylindrical cavities of inner height 1 cm and diameter 6 cm. The design simulates a compressed breast. A schematic diagram is shown in figure 1.

The cylindrical tumors and the background cylinders were filled with ^{99m}Tc such that tumor to background activity concentration ratios of 10:1 and 5:1 were achieved. The tumors were stepped through the background and imaged at each of 5 positions, or distances from the collimator face (Figure 1). Images were made with LumaGem, the single PSPMT camera and Orbiter for both activity concentration ratios. Throughout each series of images the acquisition time was adjusted to compensate for radioactive decay and where series needed to be repeated the total activity was kept constant.

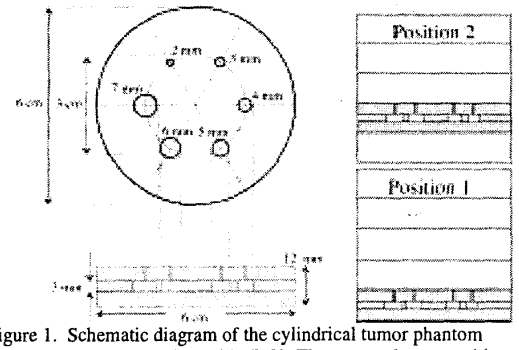

Figure 1. Schematic diagram of the cylindrical tumor phantom viewed from the top and the side (left). The tumor phantom with tumors at distances of 6 mm (position 1) and 18 mm (position 2) from the collimator face (right). Not shown are the tumors at 30 mm (position 3), 42 mm (position 4) and 54 mm (position 5) from the collimator face.

The images were evaluated by measuring the mean pixel value within a small region of interest (ROI) of constant size placed over each tumor in each image and dividing by the background pixel value to produce a tumor signal to background ratio (contrast) for each tumor size at each depth for each camera. Where possible, multiple images were taken under identical circumstances and the tumor contrast measurements were averaged together.

E. Tumor Phantom Model and Spatial Resolution

A simple mathematical model was developed to simulate imaging the cylindrical tumor phantom. Because the tumors are thin cylinders, a two dimensional projection image can be assumed. Appropriate pixel values for an ideal planar projection image are a 1.8:1 tumor to background ratio for a 10:1 activity concentration ratio. The ideal image was convolved with a two dimensional gaussian function with full width at half maximum value (FWHM) equal to the spatial resolution of the camera to create a blurred image. Noise was then added. The result is an image that represents the best a camera can possibly do under ideal circumstances, which can then be used as a measure of how well the camera is performing under realistic circumstances. This image was evaluated in the same way that the real images were.

In order to compare the model with the tumor phantom images, the overall spatial resolution was measured for each camera at distances corresponding to the depth of the tumors in background. Using these resolution values gave a model image for each camera at each tumor depth. Overall spatial resolution was measured by stepping a line source of ^{99m}Tc across the FOV and fitting a profile of the image to a gaussian function. Comparing the centroid obtained for each image with the known line source location provided a calibration factor to obtain the FHWM of the line source profile in mm. Intrinsic spatial resolution for the single PSPMT camera was measured in a similar manner but using a 0.5 mm slit in lead irradiated by ^{99m}Tc.

III. Results and Discussion

A. Fundamental Results

Energy resolution near the center of the useful FOV (UFOV) of the single PSPMT was measured to be 9.7% FWHM and 10.9% FWHM for the NaI(Tl) crystal with white and black sides, respectively. The UFOV was approximately 25 mm x 25 mm and 35 mm x 35 mm for the respective crystals. While the crystal with black sides suffers from worse energy resolution, is has a much larger UFOV. This is advantageous as the small size of the UFOV is one of the main limitations of this camera. In contrast, the UFOV for LumaGem is about 12.5 cm x 12.5 cm, and for Orbiter it is about 45 cm in diameter.

Intrinsic spatial resolution measurements are shown in table 1 for all cameras. Measurements for the single PSPMT camera were made in the uniform region of the UFOV. The data would suggest that the surface treatment of the NaI(Tl) heavily influences spatial resolution and UFOV. Overall spatial resolution measurements (with collimator) for all cameras are shown in figure 2. The single PSPMT using the NaI(Tl) crystal with white sides has the worst resolution at all collimator distances. The LumaGem camera with the hexagonal hole collimator has the best spatial resolution at all collimator distances, in spite of the fact that the hole size is larger than the hole size of the Orbiter LEHR collimator.

Table 1.

Intrinsic spatial resolution for all cameras in study at 140 keV.

	Intrinsic Spatial Resolution (Best)	Intrinsic Spatial Resolution (Mean)
Single PSPMT, NaI(Tl) white sides	3.0 mm	3.1 mm
Single PSPMT, NaI(Tl) black sides	2.0 mm	2.2 mm
Orbiter		3.5 mm
LumaGem	2 mm (Crystal Size)	2 mm (Crystal Size)

With the 2 mm matching square hole collimator, the resolution of LumaGem is severely degraded. It is comparable with Orbiter at distances close to the collimator face but falls off at larger collimator distances. The single PSPMT camera with the black sided NaI(Tl) shows improved resolution compared with Orbiter and similar resolution as the hexagonal hole LumaGem at distances less than 20 mm from the collimator face. Both the single PSPMT with black sided NaI(Tl) and LumaGem with the hexagonal hole collimator show reduced resolution with respect to Orbiter as the distance from the collimator increases.

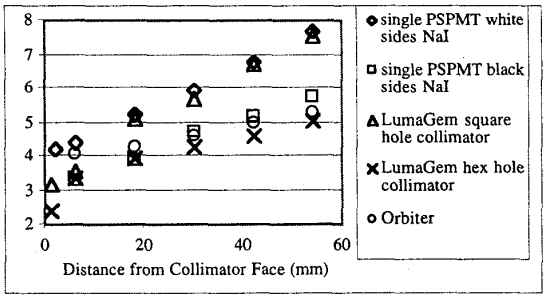

Figure 2. Overall spatial resolution in mm as a function of distance from the collimator face for three cameras and five imaging systems.

The resolution of LumaGem is expected to decrease when using the matching square hole collimator because the hole size is larger. The matching collimator, however, will improve sensitivity and it remains to be seen whether it is worth sacrificing resolution for increased sensitivity. The white coating on the sides of the continuous NaI(Tl) crystal severely degrades spatial resolution, although it increases energy resolution. This is caused by light reflecting off of the sides towards the center of the crystal, which causes severe blurring of unreflected scintillation light. The increased energy resolution and light collection with the white reflective sides are likely not enough to overcome the loss in spatial resolution and UFOV.

The observation that spatial resolution decreases for the LumaGem and PSPMT cameras relative to Orbiter as the distance from the collimator face increases is not a severe problem, as small cameras are designed to be able image at closer distances than Orbiter can, and are intended to be used to image primarily superficial tumors. For a standard compressed breast thickness of 4 cm to 6 cm, the small cameras should rarely have to image a tumor more than 2 cm to 3 cm deep in tissue. Thus, the cameras were designed with shorter than standard collimators which exhibit better resolution closer to the collimator face (that is, they have a shallow depth of field) compared with thick collimators, which better maintain their resolution at larger distances from the collimator. The use of a short collimator also has the advantage of increased sensitivity, which is essential for small FOV cameras being used in low count rate applications. The increased overall spatial resolution of small cameras is also due largely to their superior intrinsic spatial resolution.

B. Tumor Phantom Results

Results of imaging the compressed breast cylindrical tumor phantom at various depths and with various imaging systems are presented here. These are intended to evaluate imaging performance under more realistic situations, which should help to resolve some of the tradeoffs between spatial resolution, energy resolution and sensitivity discussed in the previous section. The results are also intended to compare the imaging performance of the three cameras. It is worth noting that this study is not entirely realistic, for the tumors are placed at the same distance from the collimator for each camera. In reality, Orbiter would not be able to image tumors in patients at the collimator distances in this study, whereas the LumaGem or single PSPMT would. All images evaluated in this study were processed with a 15% energy acceptance window on the (140 keV) photopeak, as is standard practice.

1) Single PSPMT Camera

Contrast is plotted for the single tube camera with the tumors at a distance of 18 mm (position 2) and 30 mm (position 3) from the collimator face in figures 3 and 4, respectively. Data are shown for the NaI crystal with white and black side coatings, both uncorrected and with the linearity correction applied.

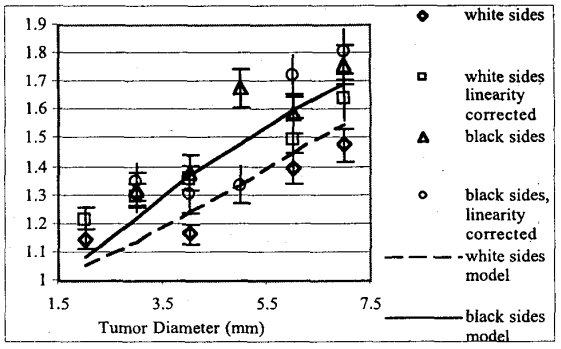

Figure 3. Single tube camera contrast is plotted vs. tumor diameter for tumors in position 2 (18 mm from the collimator face) with a 10:1 tumor to background activity concentration ratio. Data are shown as points and the mathematical model is shown as a line.

From figures 3 and 4 one can see that the black coated NaI has better contrast than the white for most tumor diameters at both distances from the collimator face. The linearity correction improves contrast somewhat in both cases. For the black coated crystal the linearity correction improves contrast only for tumor diameters 2,3,6 and 7. Tumors 4 and 5 were near the edge of the FOV and the linearity correction at that point spreads out the data so much that it had an adverse effect on the contrast. The data fit the model well in both cases, with the strange result that a few tumors exhibit higher contrast than the model. Position 1 data was not included because the black coated crystal showed anomalously high

contrast and we assumed that there must have been a problem with the acquisition or analysis that will require further investigation. Where data points are missing, the tumor was not visible to the naked eye or it was too close to the edge of the FOV to get a reliable contrast measurement.

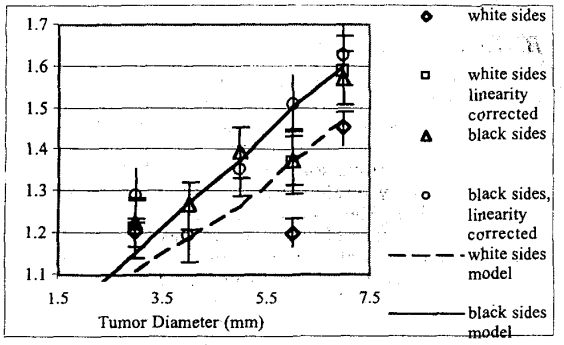

Figure 4. Single tube camera contrast is plotted vs. tumor diameter for tumors in position 3 (30 mm from the collimator face) with a 10:1 tumor to background activity concentration ratio. Data are shown as points and the mathematical model is shown as a line.

2) LumaGem Camera

Contrast is plotted for the LumaGem camera with the tumors at distances of 6 mm (position 1) and 30 mm (position 3) from the collimator in figures 5 and 6, respectively. Data are shown for both the small hexagonal hole collimator and for the square hole collimator.

It is clear from figures 5 and 6 that using the small hexagonal hole collimator on the LumaGem camera results in better tumor contrast for tumors both 6 mm and 30 mm from the collimator face. High spatial resolution seems to play a larger role in tumor detectability than sensitivity. It is interesting to note that the curves for the model have a rounded shoulder in position 1 but are relatively straight in position 3. In position 1 the tumors are close to the collimator face and scatter plays less of a role than it does at farther distances. The tumors are cylindrically shaped and thus in the absence of scatter they should have a uniform activity distribution. As the tumors get larger in the low scatter environment the difference in contrast between the center of the tumor and the background gets progressively less as the activity distribution in the tumor image becomes more and more uniform.

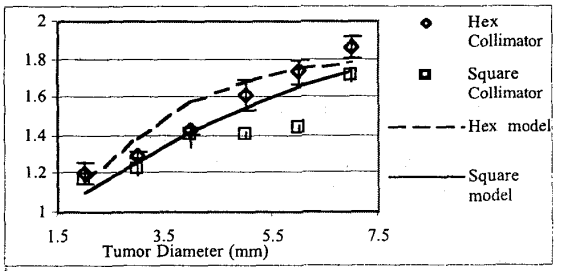

Figure 5. LumaGem Camera contrast plotted vs. tumor diameter for tumors in position 1 (6 mm from the collimator face) with a 10:1 tumor to background activity concentration ratio. Data are shown as points and the mathematical model is shown as a line.

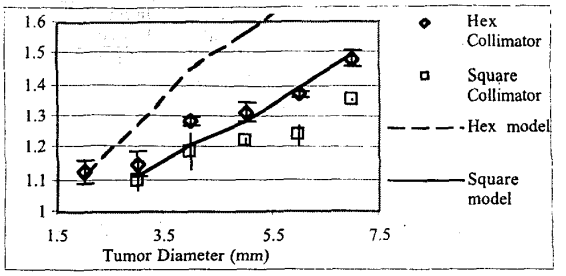

Figure 6. LumaGem Camera contrast plotted vs. tumor diameter for tumors in position 3 (30 mm from the collimator face) with a 10:1 tumor to background activity concentration ratio. Data are shown as points and the mathematical model is shown as a line.

3) Comparisons with Orbiter

Tumor contrast for all three cameras is plotted together in figures 7 and 8 with the tumors at a distance of 18

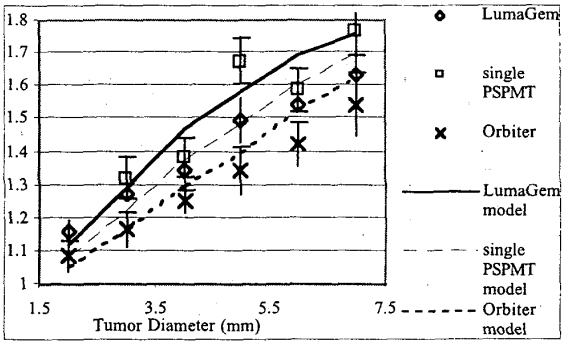

Figure 7. Contrast is plotted vs. tumor diameter for LumaGem, single PSPMT and Orbiter cameras with tumors 18 mm from the collimator face with a 10:1 tumor to background ratio.

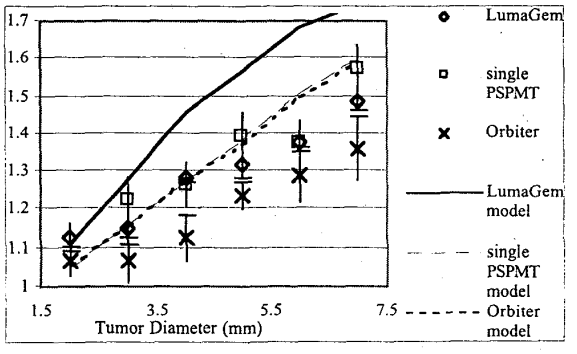

Figure 8. Contrast is plotted vs. tumor diameter for LumaGem, single PSPMT and Orbiter cameras with tumors 30 mm from the collimator face with a 10:1 tumor to background ratio.

mm and 30 mm from the collimator face, respectively. Again we show results for the 10:1 ratio. For clarity, only the "best" LumaGem and the "best" single PSPMT configurations were chosen for display. The small hexagonal hole collimator was chosen as the LumaGem representative, and the NaI with black sides was chosen as the single tube representative. We chose the uncorrected data for the inter-camera comparison because the linearity correction is not yet fully tested.

The tumor to background contrast is higher for the two small cameras compared with the Orbiter at all tumor to collimator distances. The 2 mm diameter tumor was not visible on the single PSPMT images in figures 7 and 8.

Figure 9 shows tumor to background contrast plotted for all cameras at a distance of 6 mm from the collimator face with a tumor to background ratio of 5:1.

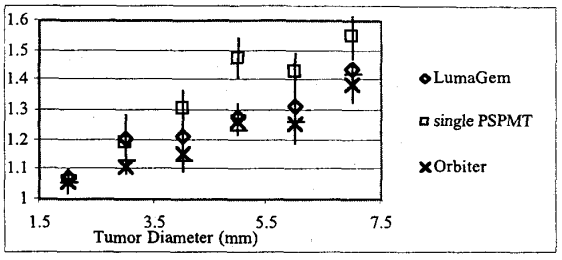

Figure 9. Contrast is plotted vs. tumor diameter for LumaGem, single PSPMT and Orbiter cameras with tumors 6 mm from the collimator face with a 5:1 tumor to background ratio.

The trend seen in figure 9 is similar to that seen in figures 7 and 8. LumaGem and the single tube do not display as high contrast values relative to Orbiter, however. Low tumor uptake values may prove to be a limiting factor in the widespread application of small, dedicated cameras.

IV. Conclusions

While many factors contribute to imaging performance and tumor contrast, it was determined that for a small continuous crystal camera it is best to wrap the sides in black absorbing material to increase the UFOV and spatial resolution. For the pixilated LumaGem camera, it was determined that spatial resolution is more important than sensitivity in tumor detection, and that the small hexagonal hole collimator should be used rather than the matching square hole collimator.

We evaluated three scintillation cameras; two compact, dedicated cameras and one large multi-purpose camera. The small cameras were found to have better intrinsic and overall spatial resolution, particularly at distances close to the collimator face. Tumor detectability studies show that for all tumor sizes at depths of up to 30 mm, the small scintillation cameras produced tumor images with a higher signal to background ratio than Orbiter. Assuming a minimum contrast level of 1.2 for reliable tumor detection, at 30 mm tumor depth in background and scatter (a tumor in the middle of a standard compressed breast), the smallest tumors detectable are 3 mm, 4 mm and 5 mm in diameter for the single continuous crystal camera, the LumaGem camera and the Orbiter camera, respectively.

V. Acknowledgements

We would like to thank the technologist staff at the UCLA Nuclear Medicine clinic for their patience and cooperation. We wish to thank Dr. Carolyn Kimme-Smith for her continued support. We also would like to thank Dr. Magnus Dahlbom and Dr. Yiping Shao for their valuable input and advice. We would like to acknowledge the help and support of Mr. Richard Liu, Mr. Alexander Pirogov, Mr. Eugene Tikhomirov, Mr. Jim Menjivar, Mr. Matt Damron, Ms. Arlyn Ramirez, and Mr. Peter Lee. This work has been funded in part by the California Breast Cancer Research Program training grant 2TB-0915 K258, by DoE Contract DE-FC03-87ER60615, and by NIH grant 5R44CA69988.

VI. References

[1] I. Khalkhali, J. A. Cutrone, I. G. Mena, L. E. Diggles, R. J. Venegas, H. I. Vargas, B. L. Jackson, S. Khalkhali, J. F. Moss, and S. R. Klein, "Scintimammography: the complementary role of Tc-99m sestamibi prone breast imaging for the diagnosis of breast carcinoma," *Radiology*, vol. 196, pp. 421-6, 1995.

[2] J. Tolmos, I. Khalkhali, H. Vargas, M. Stuntz, J. Cutrone, F. Mishkin, L. Diggles, R. Venegas, and S. Klein, "Detection of axillary lymph node metastasis of breast carcinoma with technetium-99m sestamibi scintimammography," *American Surgeon*, vol. 63, pp. 850-3, 1997.

[3] L. Maffioli, R. Agresti, A. Chiti, F. Crippa, M. Gasparini, M. Greco, and E. Bombardieri, "Prone scintimammography in patients with non-palpable breast lesions," *Anticancer Research*, vol. 16, pp. 1269-73, 1996.

[4] R. Pani, A. Soluri, R. Scafe, A. Pergola, R. Pellegrini, G. De Vincentis, G. Trotta, and F. Scopinaro, "Multi-PSPMT scintillation camera,",, 1999.

[5] D. Steinbach, S. Cherry, N. Doshi, A. Goode, B. Kross, S. Majewski, A. G. Weisenberger, M. Williams, R. Wojcik, and O. Nalcioglu, "A small scintimammography detector based on a 5" PSPMT and a crystal scintillator array,",, 1997.

[6] J. N. Aarsvold, R. A. Mintzer, N. J. Yasillo, S. J. Heimsath, T. A. Block, K. L. Matthews, X. Pan, C. Wu, R. N. Beck, C. T. Chen, and et al., "A miniature gamma camera," *Annals of the New York Academy of Sciences*, vol. 720, pp. 192-205, 1994.

[7] L. MacDonald, B. E. Patt, J. S. Iwanczyk, D. McElroy, and E. J. Hoffman, "LumaGem: High Resolution Dedicated Gamma Camera," *J Nucl Med*, vol. 41, pp. 56p, 2000.

[8] C. S. Levin, E. J. Hoffman, M. P. Tomai, and L. R. MacDonald, "PSPMT and photodiode designs of a small scintillation camera for imaging malignant breast tumors,",, 1997.

[9] C. S. Levin, E. J. Hoffman, A. K. Meadors, and M. P. Tornai, "Breast Tumor Detectability with Small Scintillation Cameras," presented at IEEE Nuclear Science Symposium and Medical Imaging Conference, Albuquerque, New Mexico, 1997.

[10] R. L. Clancy, C. J. Thompson, J. L. Robar, and A. M. Bergman, "A simple technique to increase the linearity and field-of-view in position sensitive photomultiplier tubes,",, 1997.

[11] S. E. King, F. Jih, C. B. Lim, R. Chaney, and E. Gray, "Spectral-spatial-sensitivity distortion trends and an accurate correction method in scintillation gamma cameras,",, 1985.

[12] T. K. Johnson, C. Nelson, and D. L. Kirch, "A new method for the correction of gamma camera nonuniformity due to spatial distortion," *Physics in Medicine and Biology*, vol. 41, pp. 2179-88, 1996.